Grain boundary phases in bcc metals

T. Frolov,[1] W. Setyawan,[2] R. J. Kurtz,[2] J. Marian,[3]
A. R. Oganov,[4,*] R. E. Rudd,[1] and Q. Zhu[5]

[1]*Lawrence Livermore National Laboratory, Livermore, California 94550, USA*
[2]*Pacific Northwest National Laboratory, P. O. Box 999, Richland, Washington 99352, USA*
[3]*Department of Materials Science and Engineering, University of California Los Angeles, Los Angeles, California 90095, USA*
[4]*Stony Brook University, Stony Brook, New York 11794, USA*
[5]*Department of Physics and Astronomy, High Pressure Science and Engineering Center, University of Nevada, Las Vegas, Nevada 89154, USA*

Abstract

We report a computational discovery of novel grain boundary structures and multiple grain boundary phases in elemental bcc tungsten. While grain boundary structures created by the γ-surface method as a union of two perfect half crystals have been studied extensively, it is known that the method has limitations and does not always predict the correct ground states. Here, we use a newly developed computational tool, based on evolutionary algorithms, to perform a grand-canonical search of a high-angle symmetric tilt boundary in tungsten, and we find new ground states and multiple phases that cannot be described using the conventional structural unit model. We use MD simulations to demonstrate that the new structures can coexist at finite temperature in a closed system, confirming these are examples of different GB phases. The new ground state is confirmed by first-principles calculations.

PACS numbers: 64.10.+h, 64.70.K−, 68.35.Md

Grain boundaries play a key role in the mechanical behavior of body-centered cubic (bcc) metals [1]. Their structure affects a diverse range of properties including fracture, recrystallization, and creep [2–4]. The abundance of GBs in nanocrystalline materials makes the boundaries particularly important in the class of advanced materials being developed for their promise of radiation tolerance and the combination of ductility with strength [5]. Beyond pure materials, alloy GB properties are also significant, and the GB structure can have a marked effect on segregation and morphological stability. The use of tungsten for magnetic fusion energy applications provides a noteworthy example. The ultimate success of fusion technology depends on materials that can survive the harsh operating environment. Tungsten has been selected as the divertor material in the International Thermonuclear Experimental Reactor (ITER) [6] and is a leading candidate for additional plasma-facing components in the planned follow-on tokamak DEMO [7] because of its high mechanical strength, high thermal conductivity, high melting point and low yield for sputtering. While tungsten has a number of favorable properties, it is also intrinsically brittle even at relatively high temperatures especially after recrystallization [8]. Recrystallization and intergranular fracture of tungsten impose significant design constraints. Strategies that aim to improve the ductility include alloying of the material with elements that improve the cohesion of GBs. Small amounts of added elements may have a dramatic effect on the fracture toughness of a material [3, 8–10].

One of the existing approaches to guide experimental alloy development uses atomistic calculations based on density functional theory (DFT) to screen the large space of elements in order to identify the best candidates. These DFT simulations evaluate the propensity of the system to undergo GB fracture by calculating the cleavage energy, which is the difference $\gamma_{\mathrm{GB}} - 2\gamma_{\mathrm{FS}}$ between the boundary energy and the energy of the two free surfaces [11]. Solutes segregating to different GB sites and free surfaces alter the cleavage energy resulting in increased or decreased ductility, provided the changes to the cleavage energy dominate over plasticity. DFT calculations demonstrated that segregation to different boundary sites may have opposing effects on the cleavage energy: segregation to some sites improves GB cohesion, while segregation to other sites promotes embrittlement [12]. In order to accurately predict the effect of segregation on embrittlement in these calculations it is important to evaluate the cumulative effect of segregation to many different sites. The energy of segregation to different GB sites strongly depends on the local atomic environment, i. e., the boundary structure [13–15]. Atomistic simulations also demonstrated that the kinetics of crack propagation is sensitive to grain boundary structure [16, 17].

Grain boundaries in bcc metals have been modeled using atomistic simulations for several decades [18–23]. However, in a majority of the existing studies the 0 K temperature structures were generated using the so-called γ-surface method. In this approach two misoriented perfect half-crystals are joined together while sampling different trans-

lations of the grains parallel to the GB plane. The lowest energy GB configurations are assumed to be the ground state in these calculations. During the minimization, no atoms are added or removed from the GB core. In addition, the configurational space of possible GB structures explored by the atoms during the energy minimization is rather limited.

A number of computational studies in several different materials systems demonstrated limitations of this approach and suggested that a more thorough sampling that includes the optimization of the number of atoms at the grain boundary is needed. For example, in ionic materials low-energy grain boundary structures where found when a certain fraction of ions was removed from the GB core prior to the energy minimization [24–26]. Simulated quenching to the zero-temperature limit of the grand-canonical ensemble demonstrated low-energy GB structures of a high-angle twist grain boundary in face-centered cubic (fcc) Cu with different numbers of atoms [27]. An investigation of Si twist boundaries revealed the importance of sampling and optimization of the atomic density and contrary to prior calculations demonstrated distinctly ordered ground states at 0 K [28]. Genetic algorithms designed to explore a diverse population of possible structures were applied to search for low-energy structures in symmetric tilt Si grain boundaries [29] and multicomponent ceramic grain boundaries [30].

Recent modeling in fcc metals showed that structure of relatively simple GBs with high bicrystal symmetry can be surprisingly complex and have multiple phases. Empirical potentials for Cu, Ag, Au and Ni predicted new ground states and metastable phases of several [001] symmetric tilt boundaries [31–33]. These studies systematically explored GB energetics as a function of number of atoms at the boundary. The new structures were found to have different atomic densities and complex atomic ordering with the periodic unit many times larger than that of the bulk crystals. Improved simulation methodology demonstrated first-order reversible transitions between grain boundary phases with different atomic densities triggered by temperature, changes in chemical composition and concentration of point defects [31, 33–35]. In addition, the simulations showed that at certain temperatures and chemical compositions GB phases can coexist in equilibrium with each other [31, 34]. Beyond symmetric tilt boundaries, continuous vacancy loading into general grain boundaries in Cu revealed lower energy states with different atomic density [36].

In bcc metals, recent computational studies demonstrated that changing the number of atoms in the GB core increases [37] and in some boundaries decreases GB energy [38, 39]. Little is know about phase behavior of grain boundaries in bcc metals apart from the recently found dislocation pairing transition in low-angle GBs composed of discrete dislocations [40].

The γ-surface approach remains the most commonly used method to construct GBs at 0 K, largely because no other robust computational tool of GB structure prediction

is available. On the other hand, much progress has been made in developing of computational tools to predict structures of crystals [41]. One such method is USPEX [42], which uses evolutionary algorithms to predict the structure of materials based on the compositions alone. USPEX has proved to be extremely powerful in different systems including bulk crystals [42], 2D crystals [43], surfaces [44], polymers [45] and clusters [46]. In this work we use a recently developed computational tool [33] based on the USPEX code [42, 46, 47] to explore structures and phase behavior of GBs in a bcc metal.

In this work we reexamine the structure of the symmetric tilt $\Sigma27(552)[1\bar{1}0]$ grain boundary in tungsten which is a representative high-angle boundary obtained by a 148° degree rotation of two grains around a common $[1\bar{1}0]$ tilt axis. This choice of the model system was motivated by several recent DFT studies that investigated $[1\bar{1}0]$ symmetric tilt boundaries to screen for alloying elements that would improve ductility of tungsten [12, 15, 48, 49]. In these studies the boundaries were constructed using the γ-surface method. We performed simulations of the $\Sigma27(552)[1\bar{1}0]$ using two interatomic potentials, EAM1 [50] and EAM2 [51], as well as DFT calculations [13, 52].

First, the structure of the grain boundary was generated using the γ-surface approach. The lowest energy configurations predicted by DFT calculations in Ref. [13] and the current work using the two interatomic potentials are illustrated in Fig. 1a and b, respectively. The structural units of both configurations are outlined with an orange curve to guide the eye. Notice that within the γ-surface approach, DFT and the potentials predict somewhat different structures. This result is consistent with previous studies that identified multiple metastable and energy-degenerate states generated by this methodology [38]. The view of the boundary structure along the tilt axis shown in the right-hand panel of Fig. 1 demonstrates that in both structures the atoms are confined to misoriented (110) planes of the two crystals. By construction, these GB structures can be mapped atom by atom onto a displacement symmetry conserving (DSC) lattice [1], which is the coarsest lattice that contains all of the atoms of both misoriented crystals on its lattice sites.

Second, we constructed the boundary using an evolutionary search [33] as implemented in the USPEX code [42, 46, 47]. In this approach a population of 50 to 100 different GB structures evolves over up to 50 generations by operations of heredity and mutation to predict low-energy configurations. The mutation operations include the displacements of atoms, insertion and removal of atoms from the GB core and sampling of larger-area GB reconstructions [33].

In our method, we split the bicrystal into three different regions, the upper grain (UG), the lower grain (LG), and the grain boundary (GB). UG and LG regions are taken to be 40 Å thick. The GB thickness is an input parameter predefined by the user. To ensure accurate GB energy calculation converged with respect to the system size normal to the grain boundary plane, we sandwich the GB region between two 20 Å thick buffer

regions. The atoms in the buffer zones are not affected by the evolutionary search, but can move freely during the energy minimization. We create the first generation of GB structures by randomly populating GB regions with atoms, imposing layer group symmetries [46] selected at random for each bicrystal, and then joining the three regions together applying random relative translations parallel to the grain boundary plane. The enforced symmetry is used to avoid liquid-like structures with close energies that are likely to produce similar children with poor fitness. This initial symmetry can be broken or lowered by the subsequent variation operations like heredity and mutation. The number of atoms placed in each GB slab is estimated initially from the bulk density of the perfect crystal and the thickness defined by the user. This number is then randomly varied within the interval from 0 to $N_{\mathrm{plane}}^{\mathrm{bulk}}$, where $N_{\mathrm{plane}}^{\mathrm{bulk}}$ is the number of atoms in one bulk atomic plane parallel to the GB. This ensures that structures with different atomic densities are present in the initial population. The atomic fraction [n] for each grain boundary structure is calculated according to $[n] = (N \text{ modulo } N_{\mathrm{plane}}^{\mathrm{bulk}})/N_{\mathrm{plane}}^{\mathrm{bulk}}$, where N is the total number of atoms in the GB region. We also implemented constrained searches where [n] of all GB structures in the population is within a certain interval. In the population the different bicrystals have different GB dimensions generated as random multiples of the smallest periodic GB unit [53]. The structures generated by the algorithm are relaxed externally by the LAMMPS code [54] and the grain boundary energy is determined and serves as a fitness parameter. During the optimization, the atoms in the GB region need to be fully relaxed, while the atoms in the bulk only move as rigid bodies.

Each successive generation is produced by operations of heredity and mutations, by selecting the structures with the lowest 60% of the energies as parents. In the heredity operation two grain boundary structures are randomly sliced and the parts from different parents are combined to generate the offspring. In a mutation operation the grain boundary atoms are displaced according to the stochastically picked soft vibrational modes based a bond-hardness model [46, 53]. Such mutations are advantageous to purely random displacements because they mimic a structural transition due to phonon instability upon large elastic strains and are more likely to lead to children structures with low energy. To sample different atomic densities atoms in the grain boundary region are inserted and deleted [33, 46]. The atoms are removed based on the value of the local order parameter calculated for each atom. The order parameter is described in Eq. (5) of Ref. [55]. To insert atoms into the GB slab, we identify sites unoccupied by atoms by constructing a uniform grid with a resolution of 1 $\mathrm{\AA}^3$ and fill them at random. To ensure relatively gradual changes in the GB structure, the random number of the inserted and removed atoms also does not exceed 25% of the total number of atoms in the GB slab. A more detailed description of the algorithm can be found in Ref. [33].

Figures 2 a and b illustrate the results of the evolutionary searches performed using

the EAM1 and EAM2 potentials, respectively. Each blue circle on the plot corresponds to a grain boundary structure generated during the search. The grain boundary energy is plotted as a function of the number of atoms [n] expressed as a fraction of atoms in the bulk (552) plane. The red diamonds on the plots represent the best configurations generated by the γ-surface approach. At [n]=1/2 the search with both potentials predicted new ground states of this boundary with energies 7-12% (depending on the potential) lower than that of the γ-surface generated structures. Figure 3 illustrates the structures of several [n]=1/2 GBs predicted by the two potentials. To obtain these ground states, a number of atoms equal to half (1/2) of the (552) atomic plane must be inserted into the GB core. This explains why these structures have not been discovered by the γ-surface method. The low-energy states represent 1×2 and 1×3 unit cell reconstructions and cannot be found in a standard 1×1 unit cell. At [n]=0 the EAM2 potential [51] also predicts a different low-energy GB structure, labeled as GB12, that does not require addition or removal of atoms. The boundary structure is illustrated in Fig. 4. The energy of this structure is nearly the same energy as the new ground state at the $[n] = 1/2$ atomic fraction and represents what may be a different phase of this boundary. The search with EAM2 potential clearly demonstrates that insertion or removal of atoms is not the only shortcoming of the γ-surface method: even at [n]=0 there may be distinct local minima, so prediction of grain boundary structure requires advanced sampling of many possible configurations.

The new ground states predicted by the evolutionary search are not unique. The searches with the two potentials identified about thirty distinct low-energy configurations all within a 2% energy range (approximately 0.05 J/m^2). The energies of the best thirteen configurations were subsequently refined with DFT calculations. See the Supplemental Material [56] for the details of the DFT calculations. The results of the calculations are summarized in Table 1. The DFT calculations confirmed that $[n]$=1/2 ground states predicted by both potentials have essentially the same energy. Figure 3 illustrates four examples of the ground state structures. These boundaries correspond to GBs 11, 1, 2 and 3 in Table 1. The structure in Fig. 3a was predicted by potential EAM2, while the other structures were generated using the the EAM1 potential. Each GB structure is shown from three different viewpoints. The left-hand side panel shows that all the structures are nearly indistinguishable when viewed projected on the plane normal to the $[1\bar{1}0]$ tilt axis, the standard view to visualize structural units. On the other hand, the middle and the right-hand panels show significantly different atomic arrangements. In the middle panels the tilt axis is parallel to the plane of the image, while the right-hand side panels show the structure within the GB plane viewed from the top. The top view in the right-hand side panels most clearly shows the difference between these ordered structures. In all of these configurations the atoms occupy sites between the $(1\bar{1}0)$ planes within the GB plane. These calculations show that a number

of similar structures with the same GB energy can be generated by permuting the occupancy of atoms in different *interstitial* positions within the boundary. These structures can no longer be mapped onto a DSC lattice, and to distinguish them from the structures generated by the γ-surface approach we refer to them as non-DSC structures. This characteristic feature is remarkably similar to split-kite phases recently found in [100] symmetric tilt boundaries in Cu [31], suggesting that these non-DSC structures may be a general phenomenon.

At [n]=0 the predictions of the three models are less consistent. The DFT energies of the γ-surface structures GB10 (2.960 J/m^2) and GB13 (2.973 J/m^2) generated with the empirical potentials do not agree with the energy of the γ-surface structure GB14 (2.688 J/m^2) based only on DFT. The GB12 ground state at [n]=0 predicted by the evolutionary search with EAM2 potential was also not confirmed as a low energy state by the subsequent DFT calculations. It is possible that the evolutionary search that uses DFT calculations only would generate yet a different low-energy state at [n]=0. Unfortunately, such a calculation would be significantly more expensive. Nevertheless, within the DFT model the structures GB14 at [n]=0 with energy $\gamma_{\mathrm{GB14}} = 2.68$ J/m^2 and GB1 at [n]=1/2 with energy $\gamma_{\mathrm{GB1}} = 2.592$ J/m^2 represent two candidates for distinct grain boundary phases. The close energies at 0 K suggest the possibility of transitions between the two GB structures due to temperature, pressure or alloying.

The large number of GB structures nearly degenerate in energy found by the evolutionary search at 0 K suggests new questions about tungsten grain boundaries at finite temperature. Can some of the different grain boundary structures coexist in equilibrium? How does the multiplicity of similar [n]=1/2 structures affect the finite-temperature structure? The abundance of similar structures may contribute to the configurational entropy of the boundary at finite temperature [39], since many different states can be created by permutations of atoms in different sites within the boundary with a negligible penalty in energy. To investigate the effect of temperature on [n]=1/2 GB structure, we performed a molecular dynamics simulation for 100 ns at high temperature (2500 K) with the EAM1 potential. To avoid bias for one of the newly identified [n]=1/2 ground states, we used a higher-energy structure predicted by the γ-surface approach (Fig. 1b) as the initial configuration. Along the x direction we terminated the GB with two $(\bar{1}15)$ surfaces to allow atoms to diffuse in and out, enabling the atomic density in the GB core to vary [31]. During the simulation, the GB transforms to its non-DSC state. The equilibrium high-temperature structure is illustrated in Fig. 5. The simulation confirms that the non-DSC ground state identified by the evolutionary search remains the minimum free energy structure at high temperature. The examination of the boundary structure viewed from the top in Fig. 5b reveals that the high-temperature structure is a combination of different structures shown in Figs. 3c and d [39, 57]. The left surface shows a *chevron* reconstruction [58, 59]. Near the chevron the first two GB units have a different

structure closely resembling the [n]=0 non-DSC ground state GB12 identified using the EAM2 potential. This example also shows that the GB structure in a polycrystalline metal will be influenced by local mechanical forces (e.g. triple junctions, GB defects, nearby lattice dislocations, etc.)

The evolutionary search with the EAM2 potential predicts two distinct low-energy structures with [n]=0 and [n]=1/2. MD simulations of the individual structures at T=2000 K and T=2500 K with periodic boundary conditions confirmed that both are stable at finite temperature. To test whether the two types of structures can coexist we created a simulation block with dimensions $49.5 \times 2.7 \times 13.0$ nm^3 and periodic boundary conditions along the boundary. The initial GB structure was set to GB12. Then, additional atoms were inserted at random positions in one half of the bicrystal at a distance 5 to 10 Å above the GB plane. The number of atoms inserted in that section of the block was equal to half of a (552) atomic plane. This configuration was annealed at 2000 K for 200 ns. During the first few nanoseconds of the simulation the added atoms diffused into the GB and about half of the total GB area transformed into the [n]=1/2 structure. After that, the two grain boundary structures continued to coexist for the rest of the simulation time and we observed no further transformations. Figure 6 illustrates the [n]=0 and [n]=1/2 grain boundary phases coexisting in equilibrium. The two structures are separated by a line defect that spans the periodic length of the simulation block. The position of this line defect fluctuates during the simulation. The equilibrium in this closed system with periodic boundary conditions is established by exchange of atoms diffusing along the boundary. The coexistence simulation demonstrate that the two types of structures predicted by the evolutionary search represent two GB phases. The transformation is first-order and results in a discontinuous change in excess GB properties. This is to be contrasted to higher order transitions such as continuous premelting when only one GB state can exist at given temperature and pressure. To the best of our knowledge this is a first demonstration of phase behavior of high-angle GBs in a bcc material.

In conclusion, conventional simulation methodologies such as the γ-surface method often predict relatively simple structures for symmetric tilt boundaries, which are composed of kite-shaped units such as illustrated in Fig. 1. Their structure can be described within the structural unit model which is based on bulk crystallography [38]. For this reason symmetric tilt boundaries are considered to be some of the simplest boundaries, and they are popular model systems. In this work we have demonstrated that in bcc material such as tungsten, the structure of symmetric tilt boundaries can be significantly more complex.

We performed a grand-canonical evolutionary structure search of the $\Sigma27(552)[1\bar{1}0]$ boundary; i.e. a search in which the number of atoms can vary. This boundary has been investigated in the past to study solute segregation and GB embrittlement [13, 52]. Our

calculations with two different interatomic potentials and DFT predict a new ground state, which requires additional atoms equivalent to half of a (552) atomic plane. The lack of atomic density optimization and the absence of sufficient sampling are the two main reasons this ground state was not found previously.

The new ground state structures are characterized by complex arrangement of atoms within the GB plane. The boundaries are composed of a number of atoms incompatible with the number of atoms per atomic plane in the abutting grains. The GB structure cannot be mapped onto the DSC lattice. The ground state is degenerate, represented by a large number of similar structures with the same energy. This configurational complexity has consequences for the finite-temperature GB structure, which we observe to be comprised of a combination of states found at 0 K. The structural features are remarkably similar to split-kite phases found in symmetric tilt fcc GBs [31, 33].

Within the EAM2 model the evolutionary search at 0 K identified two distinct low-energy GB structures with different atomic densities [n]=0 and [n]=1/2. High-temperature MD simulations demonstrated that the two structures can coexist in equilibrium in a closed system while exchanging atoms by diffusion. This simulation confirms that the two structures are examples of two GB phases. Within the DFT model the energy difference between the different structures GB14 and GB1 is only 3%. The closeness of the energies at 0 K also suggests a possibility of transitions between the two GB structures due to temperature, pressure or addition of solute atoms.

Transformations at grain boundaries are not only of fundamental scientific interest, but may also have practical importance by affecting the properties of materials. A number of recent experimental studies demonstrated discontinuous changes in properties of polycrystalline materials and bicrystals, linking grain boundary phase transitions to abnormal grain growth, activated sintering and grain boundary embrittlement [3, 60–65]. Multiple GB phases found by atomistic simulations in fcc Cu provided a convenient model to investigate the importance of GB structure-property relations. Specifically, the simulations revealed that the transitions between these GB structures have a pronounced effect on shear strength and can even reverse the direction of GB migration [66, 67]. In a binary Cu(Ag) system, the different GB phases demonstrated distinct monolayer and bilayer segregation patterns with very different amounts of Ag segregation [32, 35]. In other words, the changes in GB structure can dramatically alter the segregation sites and the occupation of these sites by solutes.

In this work we demonstrated new ground states and phase behavior of grain boundaries in a model bcc metal. In our high-temperature simulations the GB transition (the nucleation of the second GB phase) was triggered by absorption of interstitial atoms. This mechanism of defect accommodation by GBs may be relevant to higher radiation tolerance of nanocrystalline materials. The detailed investigation of impurity segregation to non-DSC grain boundaries and their mechanical properties is the subject of

Label	$[n]$	EAM1, J/m^2	EAM2, J/m^2	DFT, J/m^2
GB1	1/2	2.819		2.592
GB2	1/2	2.811		2.593
GB3	1/2	2.818		2.594
GB4	1/2	2.807		2.595
GB5	1/2	2.817		2.609
GB6	1/2	2.802		2.610
GB7	1/2	2.798		2.624
GB8	1/2	2.796		2.626
GB9	1/2	2.812		2.628
GB10*	0	3.171		2.960
GB11	1/2		2.493	2.590
GB12	0		2.495	2.951
GB13*	0		2.670	2.973
GB14*	0			2.680

Table I. The grain boundary energy of different structures generated with the evolutionary algorithm and the γ-surface approach (*) using the EAM1 and EAM2 potentials and DFT. The second column indicates the atomic density $[n]$ of the different structures as a fraction of the atoms in the (552) plane. Both potentials predict new ground states that were found with the grand-canonical evolutionary search. The ground state is represented by several similar but distinct structures with the same energy within the accuracy of the DFT calculations. GB14 was previously found in Ref. [13].

future work. The rich behavior found in a high-angle and high-energy $\Sigma27(552)[1\bar{1}0]$ grain boundary using the new evolutionary method motivates a systematic investigation of other grain boundaries in bcc metals as well as grain boundary phase transitions in tungsten alloys.

ACKNOWLEDGMENT

This work was performed under the auspices of the U.S. Department of Energy (DOE) by Lawrence Livermore National Laboratory under contract DE-AC52-07NA27344 and by Pacific Northwest National Laboratory under contract DE-AC05-76RLO-1830. This material is based upon work supported by the U.S. DOE, Office of Science, Office of Fusion Energy Sciences. The work was supported by the Laboratory Directed Research and Development Program at LLNL, project 17-LW-012. We acknowledge the use of LC computing resources. Work in UNLV is supported by the National Nuclear Security

Administration under the Stewardship Science Academic Alliances program through DOE Cooperative Agreement DE-NA0001982.

---

* Current address: Skolkovo Institute of Science and Technology, Skolkovo Innovation Center, 3 Nobel St., Moscow 143026, Russia

[1] A. P. Sutton and R. W. Balluffi, *Interfaces in Crystalline Materials*, Clarendon Press, Oxford, 1995.

[2] M. P. Harmer, Journal of the American Ceramic Society **93**, 301 (2010).

[3] J. Luo, H. Cheng, K. M. Asl, C. J. Kiely, and M. P. Harmer, Science **333**, 1730 (2011).

[4] Symbols, in *Recrystallization and Related Annealing Phenomena (Second Edition)*, edited by F. Humphreys and M. Hatherly, pages xxi – xxii, Elsevier, Oxford, second edition edition, 2004.

[5] K. Lu, L. Lu, and S. Suresh, Science **324**, 349 (2009).

[6] S. Zinkle and L. Snead, Annual Review of Materials Research **44**, 241 (2014).

[7] D. Maisonnier, D. Campbell, I. Cook, L. D. Pace, L. Giancarli, J. Hayward, A. L. Puma, M. Medrano, P. Norajitra, M. Roccella, P. Sardain, M. Tran, and D. Ward, Nuclear Fusion **47**, 1524 (2007).

[8] Y. Mutoh, K. Ichikawa, K. Nagata, and M. Takeuchi, J. of Mat. Sci. **30**, 770 (1995).

[9] M. K. Miller and A. J. Bryhan, Materials Science and Engineering: A **327**, 80 (2002).

[10] T. G. Nieh, Scripta Metallurgica **18**, 1279 (1984).

[11] J. R. Rice and J.-S. Wang, Materials Science and Engineering: A **107**, 23 (1989).

[12] W. Setyawan and R. J. Kurtz, Scripta Materialia **66**, 558 (2012).

[13] W. Setyawan and R. J. Kurtz, Journal of Physics: Condensed Matter **26**, 135004 (2014).

[14] D. Scheiber, V. I. Razumovskiy, P. Puschnig, R. Pippan, and L. Romaner, Acta Materialia **88**, 180 (2015).

[15] X. Wu, Y.-W. You, X.-S. Kong, J.-L. Chen, G. N. Luo, G.-H. Lu, C. S. Liu, and Z. Wang, Acta Materialia **120**, 315 (2016).

[16] G. Schoeck and W. Pichl, Phys. Status Solidi A **118**, 109 (1990).

[17] J. J. Moller and E. Bitzek, Acta Materialia **73**, 1 (2014).

[18] K. Morita and H. Nakashima, Materials Science and Engineering: A **234**, 1053 (1997).

[19] M. A. Tschopp, K. N. Solanki, F. Gao, X. Sun, M. A. Khaleel, and M. F. Horstemeyer, Phys. Rev. B **85**, 064108 (2012).

[20] D. Wolf, Philosophical Magazine Part B **59**, 667 (1989).

[21] D. Wolf, Journal of Applied Physics **69**, 185 (1991).

[22] D. Yeşilleten and T. A. Arias, Phys. Rev. B **64**, 174101 (2001).

[23] S. Ratanaphan, D. L. Olmsted, V. V. Bulatov, E. A. Holm, A. D. Rollett, and G. S. Rohrer, Acta Materialia **88**, 346 (2015).

[24] P. W. Tasker and D. M. Duffy, Philos. Mag. A **47**, L45 (1983).

[25] D. M. Duffy and P. W. Tasker, Philos. Mag. A **53**, 113 (1986).

[26] D. M. Duffy and P. W. Tasker, J. Am. Ceram. Soc **67**, 176 (1984).

[27] S. R. Phillpot and J. M. Rickman, The Journal of Chemical Physics **97**, 2651 (1992).

[28] S. von Alfthan, P. D. Haynes, K. Kashi, and A. P. Sutton, Phys. Rev. Lett. **96**, 055505 (2006).

[29] J. Zhang, C.-Z. Wang, and K.-M. Ho, Phys. Rev. B **80**, 174102 (2009).

[30] A. L. S. Chua, N. A. Benedek, L. Chen, M. W. Finnis, and A. P. Sutton, Nat Mater **9**, 418 (2010).

[31] T. Frolov, D. L. Olmsted, M. Asta, and Y. Mishin, Nat. Commun. **4**, 1899 (2013).

[32] T. Frolov, S. V. Divinski, M. Asta, and Y. Mishin, Phys. Rev. Lett. **110**, 255502 (2013).

[33] Q. Zhu, A. Samanta, B. Li, R. E. Rudd, and T. Frolov, arXiv:1707.09699.

[34] T. Frolov, M. Asta, and Y. Mishin, Curr. Opin. Solid State Mater. Sci. **20**, 308 (2016).

[35] T. Frolov, M. Asta, and Y. Mishin, Phys. Rev. B **92**, 020103 (2015).

[36] W. Yu and M. Demkowicz, Journal of Materials Science **50**, 4047 (2015).

[37] I. Novoselov and A. Yanilkin, Computational Materials Science **112, Part A**, 276 (2016).

[38] J. Han, V. Vitek, and D. J. Srolovitz, Acta Materialia **133**, 186 (2017).

[39] J. Han, V. Vitek, and D. J. Srolovitz, Acta Mater. **104**, 259 (2016).

[40] D. L. Olmsted, D. Buta, A. Adland, S. M. Foiles, M. Asta, and A. Karma, Phys. Rev. Lett. **106**, 046101 (2011).

[41] A. M. Reilly et al., Acta Crystallographica Section B **72**, 439 (2016).

[42] A. R. Oganov and C. W. Glass, The Journal of Chemical Physics **124**, 244704 (2006).

[43] X.-F. Zhou, X. Dong, A. R. Oganov, Q. Zhu, Y. Tian, and H.-T. Wang, Phys. Rev. Lett. **112**, 085502 (2014).

[44] Q. Zhu, L. Li, A. R. Oganov, and P. B. Allen, Phys. Rev. B **87**, 195317 (2013).

[45] Q. Zhu, V. Sharma, A. R. Oganov, and R. Ramprasad, The Journal of Chemical Physics **141**, 154102 (2014).

[46] A. O. Lyakhov, A. R. Oganov, H. T. Stokes, and Q. Zhu, Computer Physics Communications **184**, 1172 (2013).

[47] A. R. Oganov, A. O. Lyakhov, and M. Valle, Accounts of Chemical Research **44**, 227 (2011).

[48] D. Scheiber, R. Pippan, P. Puschnig, and L. Romaner, Modelling and Simulation in Materials Science and Engineering **24**, 085009 (2016).

[49] Z. W. Li, X. S. Kong, Liu-Wei, C. S. Liu, and Q. F. Fang, Chinese Physics B **23**, 106107 (2014).

[50] M. C. Marinica, L. Ventelon, M. R. Gilbert, L. Proville, S. L. Dudarev, J. Marian, G. Bencteux, and F. Willaime, Journal of Physics: Condensed Matter **25**, 395502 (2013).

[51] X. Zhou, H. Wadley, R. Johnson, D. Larson, N. Tabat, A. Cerezo, A. Petford-Long, G. Smith, P. Clifton, R. Martens, and T. Kelly, Acta Materialia **49**, 4005 (2001).

[52] W. Setyawan and R. J. Kurtz, Journal of Physics: Condensed Matter **26**, 135004 (2014).

[53] Q. Zhu, A. R. Oganov, A. O. Lyakhov, and X. Yu, Phys. Rev. B **92**, 024106 (2015).

[54] S. Plimpton, J. Comput. Phys. **117**, 1 (1995).

[55] A. O. Lyakhov, A. R. Oganov, and M. Valle, Comput. Phys. Commun. **181**, 1623 (2010).

[56] See supplemental material at [url] for complete results of the evolutionary search search, the details of the dft calculations and the atomic structure of GB12.

[57] R. G. Hoagland and R. J. Kurtz, Philos. Mag. A **82**, 1073 (2002).

[58] F. Lançon, T. Radetic, and U. Dahmen, Phys. Rev. B **69**, 172102 (2004).

[59] T. Radetic, F. Lançon, and U. Dahmen, Phys. Rev. Lett. **89**, 085502 (2002).

[60] M. Baram, D. Chatain, and W. D. Kaplan, Science **332**, 206 (2011).

[61] M. P. Harmer, Science **332**, 182 (2011).

[62] W. Rheinheimer and M. J. Hoffmann, Scripta Materialia **101**, 68 (2015).

[63] P. R. Cantwell, M. Tang, S. J. Dillon, J. Luo, G. S. Rohrer, and M. P. Harmer, Acta Materialia **62**, 1 (2014).

[64] J. D. Schuler and T. J. Rupert, Acta Materialia **140**, 196 (2017).

[65] G. S. Rohrer, Curr. Opin. Solid State Mater. Sci. **20**, 231 (2016).

[66] T. Frolov, Appl. Phys. Lett. **104**, 211905 (2014).

[67] V. Borovikov, X.-Z. Tang, D. Perez, X.-M. Bai, B. P. Uberuaga, and A. F. Voter, Journal of Physics: Condensed Matter **25**, 035402 (2013).

[68] A. Stukowski, Modell. Simul. Mater. Sci. Eng. **18**, 015012 (2010).

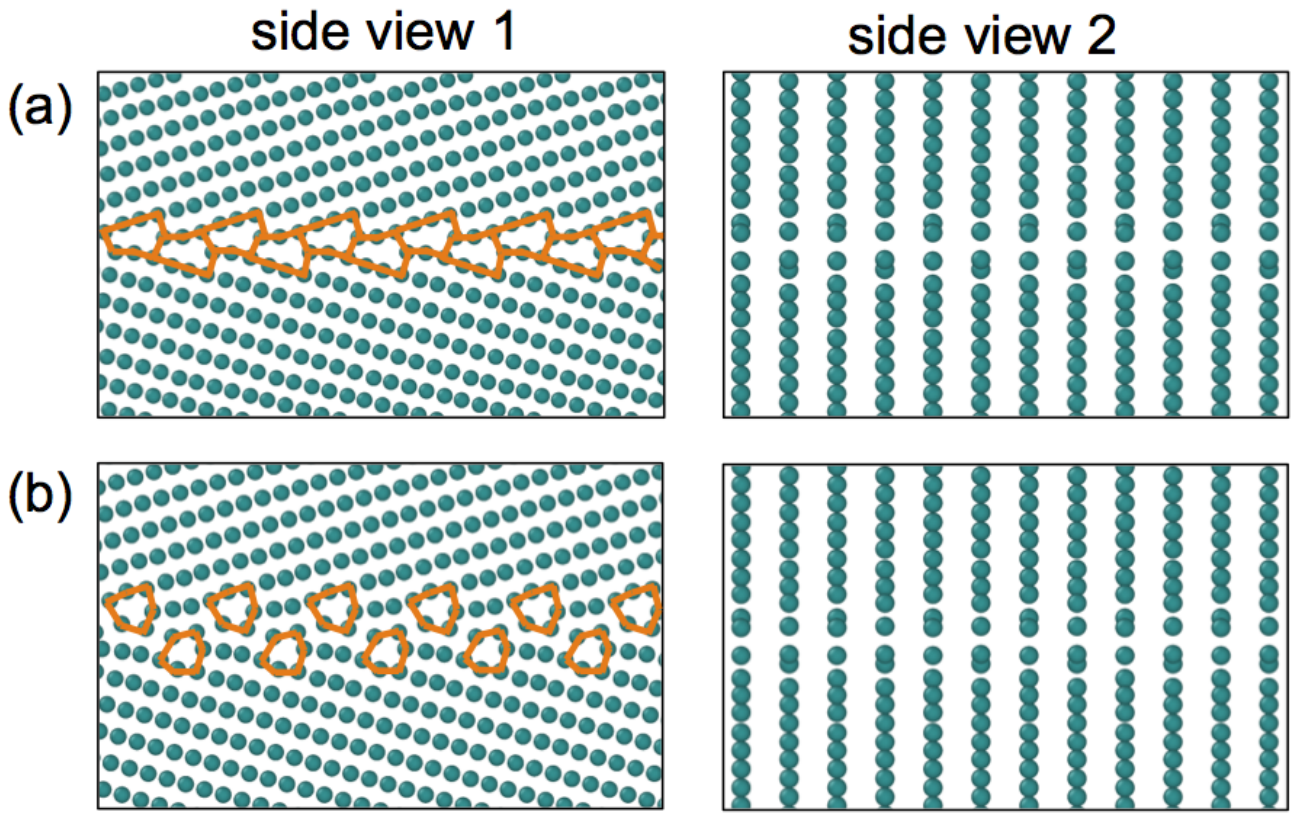

Figure 1. Conventional methodology: γ-surface constructed $\Sigma 27(552)[1\bar{1}0]$ GB in W using (a) DFT [13] and (b) the EAM1 [51] and EAM2 [50] potentials.

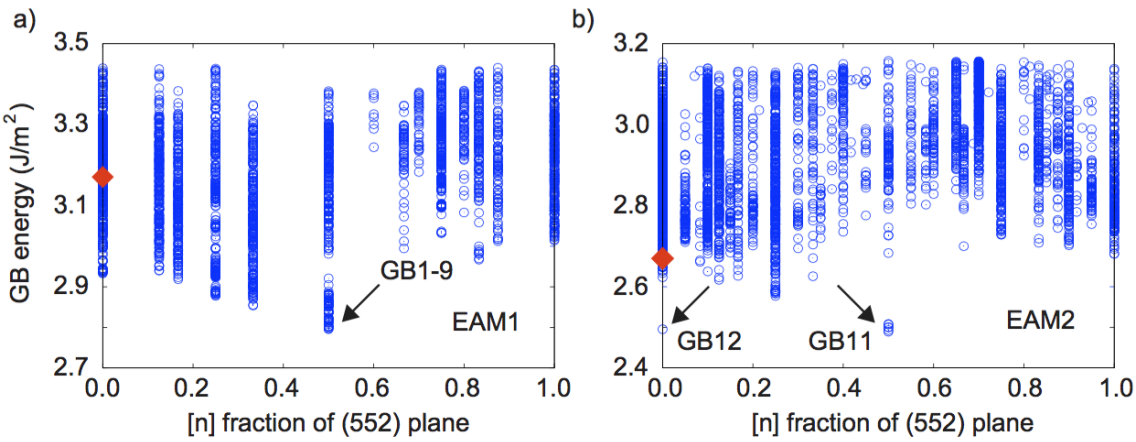

Figure 2. Results of the evolutionary search. The grain boundary energy for different structures of the $\Sigma 27(552)[1\bar{1}0]$ boundary in W generated by the evolutionary search with (a) the EAM1 [50] and (b) EAM2 [51] potentials. The energy is plotted as a function of the number of atoms [n] expressed as a fraction of atoms in the (552) plane. The red diamonds on the plots represent the best configurations generated by the conventional γ-surface approach. The arrows point to new ground states with different atomic densities predicted by the evolutionary search.

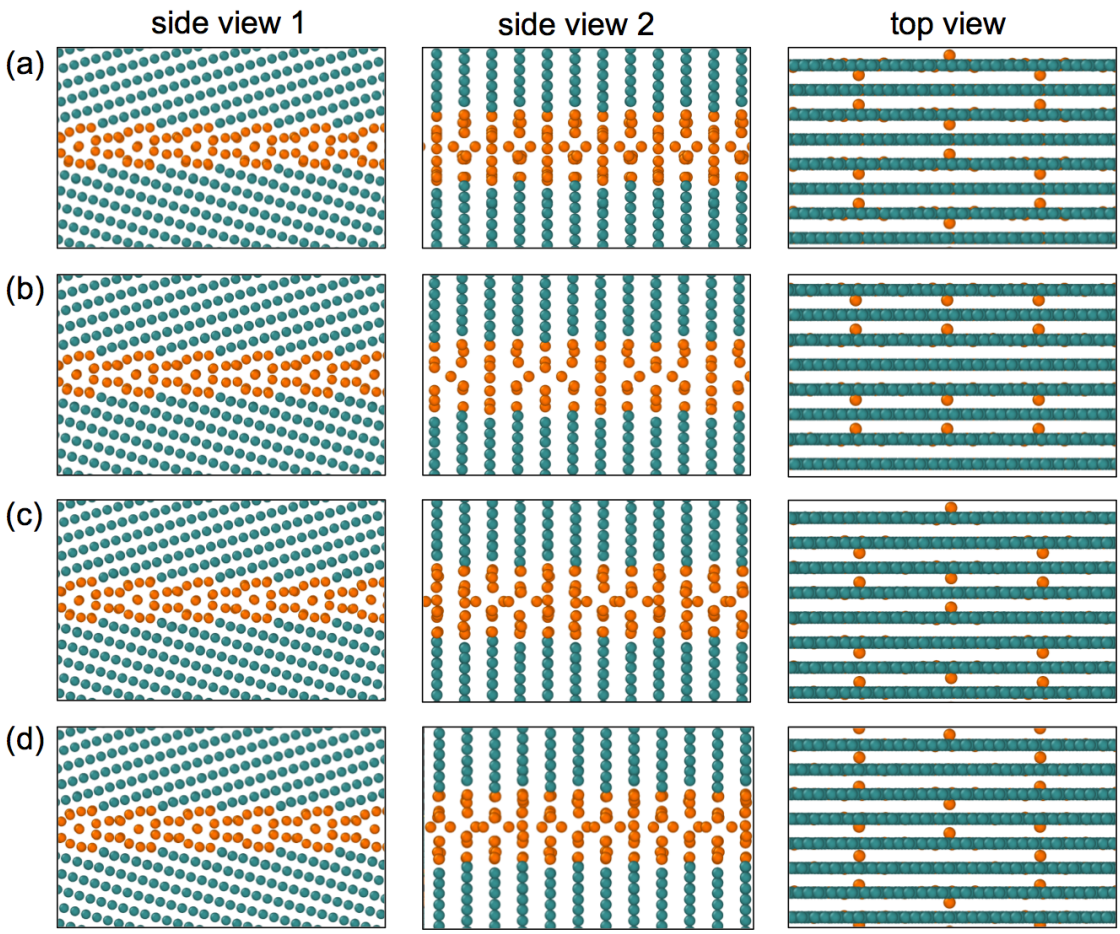

Figure 3. New [n]=1/2 ground state structures of the $\Sigma 27(552)[1\bar{1}0]$ GB in W predicted by the evolutionary structure search with the EAM1 [50] and EAM2 [51] potentials: (a) GB11, (b) GB1, (c) GB2 and (d) GB3. The DFT calculations confirm these to be the lowest energy states with the energies $\gamma_{\mathrm{GB}} = 2.59$ J/m^2 identical within the accuracy of the calculations. Bulk (green) and grain boundary (orange) atoms are colored according to the common neighbor analysis [68].

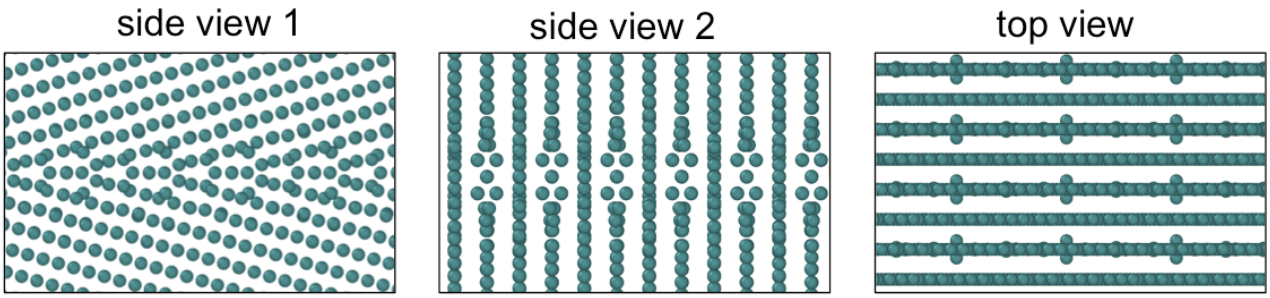

Figure 4. GB12 structure of the $\Sigma 27(552)[1\bar{1}0]$ GB in W predicted by the evolutionary search at $[n]_{\mathrm{GB12}} = 0$ with the EAM2 potential [51]. The energy of this structure $\gamma_{\mathrm{GB12}} = 2.495$ J/m^2 is identical within the accuracy of the calculations to the energy of the ground state structure GB11 with $\gamma_{\mathrm{GB11}} = 2.493$ J/m^2 and $[n]_{\mathrm{GB11}} = 1/2$ (cf. Fig. 3a). This structure has the same number of atoms as the γ-surface structure, but the energy is 7% lower. In this case no atoms were inserted or removed from the GB core, however the evolutionary search finds this low-energy structure by rearranging the GB atoms.

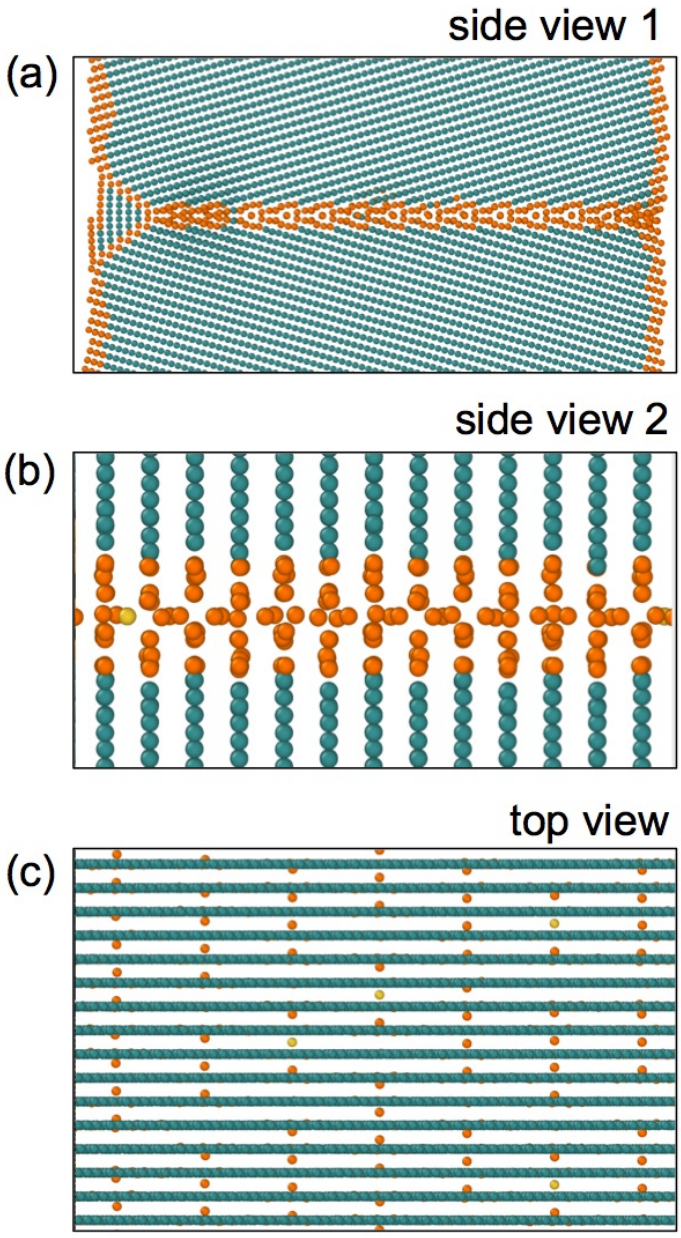

Figure 5. Equilibrium structure of the $\Sigma 27(552)[1\bar{1}0]$ GB at T=2500 K modeled with the EAM1 potential. A 100 ns long isothermal molecular dynamic simulation with the GB terminated at two open surfaces predicts the high-temperature GB stucture independently from the 0 K search. Bulk (green) and grain boundary (orange) atoms are colored according to the common neighbor analysis [68].

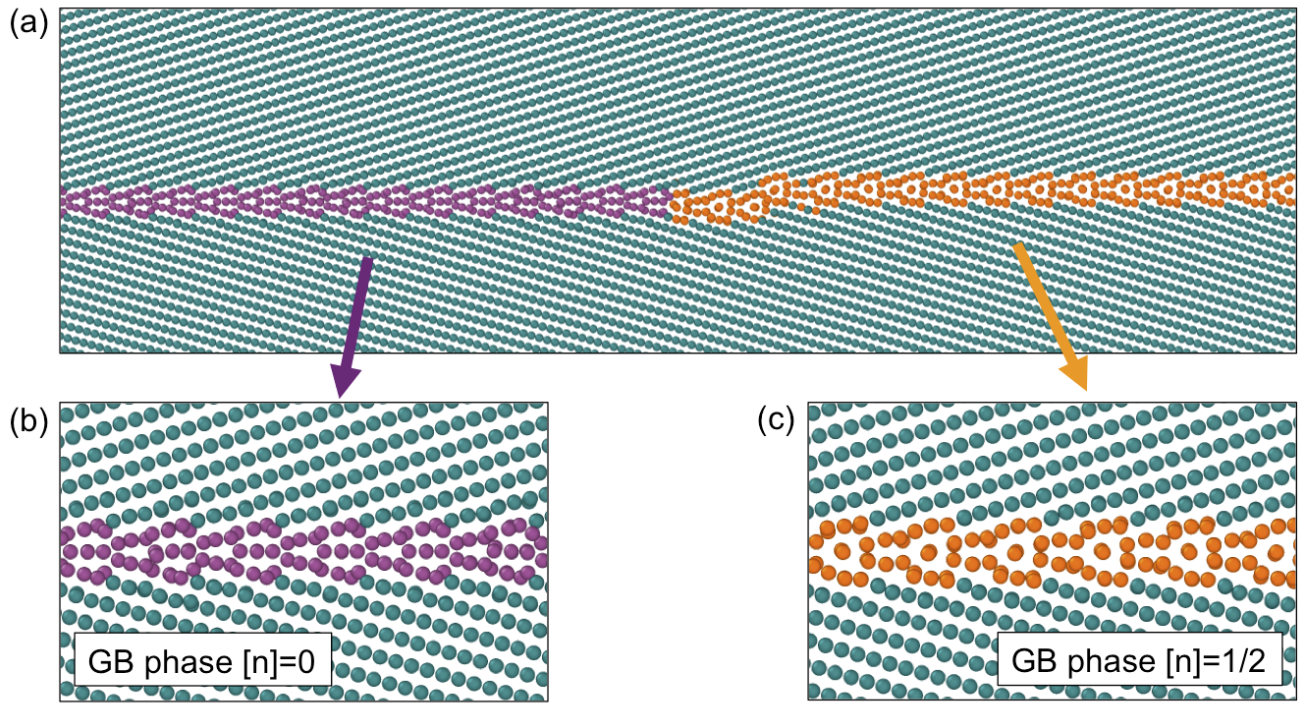

Figure 6. (a) Two grain boundary phases [n]=0 and [n]=1/2 coexisting in equilibrium at T=2000 K for 200 ns in a closed system with periodic boundary conditions along the boundary. b) and c) show closer views of the two structures. The equilibrium is established through the exchange of atoms bethween the two GB phases. The coexistence simulation demonstrates that the two types of structres predicted by the evolutionary search at 0 K represent two different GB phases. The γ-surface approach fails to predict both of these finite-temperature structures. In the figure the bulk (green) and the grain boundary (orange, magenta) atoms are colored according to the common neighbor analysis [68].